J Appl Electrochem (2016) 46:667–677
DOI 10.1007/s10800-016-0955-z

RESEARCH ARTICLE

Nitrogen-containing chitosan-based carbon as an electrode material for high-performance supercapacitors

Agata Śliwak[1] · Noel Díez[1] · Ewa Miniach[1] · Grażyna Gryglewicz[1]

Received: 6 November 2015 / Accepted: 14 March 2016 / Published online: 22 March 2016

Abstract Nitrogen-containing activated carbons were prepared from chitosan, a widely available and inexpensive biopolysaccharide, by a simple procedure and tested as electrode material in supercapacitors. The physical activation of chitosan chars with CO_2 led to carbons with a very high nitrogen content (up to 5.4 wt%) and moderate surface areas (1000–1100 m^2 g^{-1}). Only chitosan-based activated carbons with a similar microporous structure were considered in this study to evaluate the effect of the nitrogen content and distribution on their electrochemical performance. The N-containing activated carbons were tested in two- and three-electrode supercapacitors using an aqueous electrolyte (1 M H_2SO_4), and they exhibited superior surface capacitance (19.5 μF cm^{-2}) and pseudocapacitance compared to a commercial activated carbon with a negligible nitrogen content and similar microporosity. The low oxygen content and the presence of stable quaternary nitrogen improved the charge propagation on the chitosan-based carbons, which was confirmed by the high capacity retention of 83 %. The chitosan-based carbons exhibited excellent cyclic stability and maintained 100 % of their capacitance after 5000 charge/discharge cycles at a current density of 1 A g^{-1}. These results demonstrate the suitability of chitosan-based carbons for application in energy storage systems.

Electronic supplementary material The online version of this article (doi:10.1007/s10800-016-0955-z) contains supplementary material, which is available to authorized users.

✉ Grażyna Gryglewicz
grazyna.gryglewicz@pwr.edu.pl

[1] Department of Polymer and Carbonaceous Materials, Faculty of Chemistry, Wrocław University of Technology, Gdańska 7/9, 50-344 Wrocław, Poland

Graphical Abstract

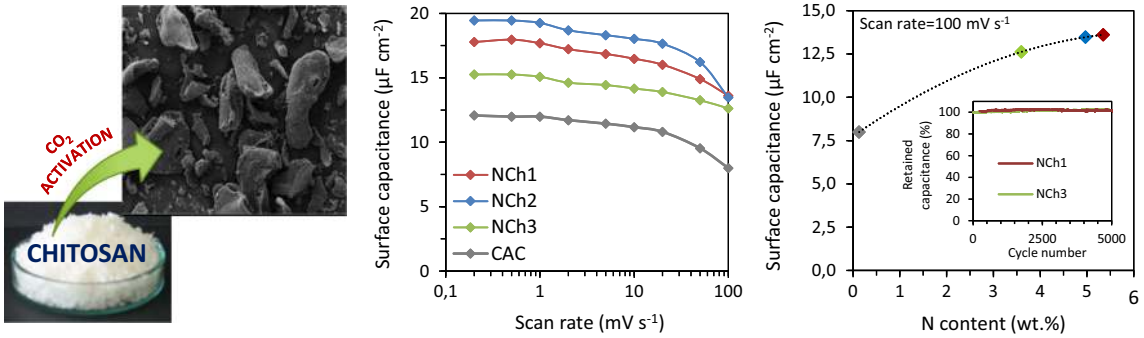

Chitosan-based activated carbons were characterized by excellent rate capabilities and high capacitance values due to their high content of stable nitrogen functionalities

Keywords Chitosan · CO_2 activation · Nitrogen-doped porous carbon · Pseudocapacitance · Supercapacitor

1 Introduction

Electrochemical double-layer capacitors (EDLCs), which are also known as supercapacitors or ultracapacitors, are energy storage devices that have attracted extensive attention in scientific and industrial fields during the last decade due to their high power capability, fast energy delivery, short charging time, and good cyclability [1]. Among the different materials studied as electrodes for supercapacitors, activated carbons (ACs) are the most widely used due to their high surface area and relatively low resistivity [2, 3]. Because the main energy storage mechanism in EDLCs arises from the electrostatic accumulation of electrolyte ions on the electrode surface, the capacitance of EDLCs typically increases with the specific surface area of the ACs [4, 5]. Highly porous materials with specific surface areas exceeding 3000 $m^2\ g^{-1}$ have been obtained by KOH activation of carbons [6–9], but commercially available ACs typically exhibit a more modest porosity of approximately 1000–1500 $m^2\ g^{-1}$.

The capacitive behavior of ACs can be significantly enhanced by the incorporation of heteroatoms into the carbon framework, due to faradaic redox reactions between the electrode material and the electrolyte. Therefore, tailoring the porous structure and the surface chemistry of carbon materials to optimize their electrochemical behavior remains challenging. Specifically, the presence of nitrogen not only provides pseudocapacitance but also increases the electron-donor capability of the N-enriched carbons [10–12]. Several post-activation techniques, such as ammoxidation, amination, and treatment with nitrogen-containing organic compounds, have been employed to enrich AC surfaces with nitrogen [11, 13–16]. The use of nitrogen-containing carbon precursors appears to be more desirable because it avoids the use of post-treatments and guarantees a uniform distribution of nitrogen atoms in the bulk of the material [17]. The preparation of ACs from various N-enriched carbon precursors, including polymers, as well as their electrochemical behavior, has been previously reported [18–23]. In addition, good correlations between capacitance and nitrogen content have been observed [7].

Chitosan is an N-containing biopolysaccharide that has been extensively applied in medicine, the food industry, and water treatment. Chitosan is the deacetylated form of chitin, which is the second most abundant biopolymer after cellulose. Because chitin is produced in huge amounts as a by-product in the food industry, its use as a precursor for carbon materials is interesting from economic and environmental perspectives. The preparation of ACs by the chemical activation of chitosan chars using Na_2CO_3, K_2CO_3, $ZnCl_2$, or KOH as activating agents has been reported [24–29]. However, only limited investigations of their use as electrode materials for supercapacitors have been reported. KOH-activated chitosan chars with specific surface areas as high as 3500 $m^2\ g^{-1}$ exhibited capacitance values as high as 221 F g^{-1} at 1 A g^{-1} in a three-electrode cell in a 6 M KOH electrolyte, with a capability retention of 89 % after 1000 cycles [28]. Although a good correlation was observed between the Brunauer–Emmett–Teller (BET) surface area and the specific capacitance, the presence of nitrogen and its effect on the capacitive behavior was not discussed, which is most likely due to the fast release of nitrogen during the chemical activation with KOH. The preparation of the nitrogen-doped AC from prawn shells for the use as electrode in supercapacitors has been recently reported [29]. This material, containing 4 wt% of nitrogen, was highly oxidized (reaching 21 wt% of oxygen) due to the KOH activation used for the preparation of the porous carbons. A very high capacitance value of 380 F g^{-1} was obtained at a current density of 1 A g^{-1}

in a 1 M H_2SO_4 electrolyte which seems most likely arises from the pseudocapacitance due to a very high heteroatom content. However, the individual effect of the nitrogen content and its contribution to the capacity retention at high current densities was not evaluated. Our study shows that physical activation of chitosan chars with CO_2 enables to prepare N-doped ACs with low oxygen content, while this activation route also avoids the use of hazardous chemicals and the subsequent washing steps.

In this study, chitosan-based ACs with a moderate surface area (1000 m^2 g^{-1}) and a high nitrogen content (3.6–5.4 wt%) were obtained by the CO_2 activation of chitosan chars. The comparison of N-containing ACs with similar porous textures allowed us to determine the effects of the nitrogen content and the distribution of nitrogen groups on the capacitive behavior. The high nitrogen content resulted in a pseudocapacitance effect and an increase in the capacitance, which was maintained after 5000 cycles at 1 A g^{-1}. The improved conductivity and high-rate capability were related to the high content of quaternary nitrogen.

2 Materials and methods

2.1 Preparation of chitosan-based ACs

Three different chitosans purchased from Sigma-Aldrich were used as N-enriched carbon precursors (Ch1, from crab shells in the form of flakes; Ch2, ground flakes and powder; Ch3, powder). The nitrogen content in the chitosan samples was very similar, i.e., 8.1–8.3 wt%. The chitosan chars were prepared by placing 5–7 grams of chitosan into a quartz boat, followed by heating to 900 °C in a horizontal furnace under a nitrogen flow of 20 dm^3 h^{-1}. Carbonization was conducted at a heating rate of 5 °C min^{-1} with a soaking time of 15 min at the final temperature. The elemental composition of the chitosans and their obtained chars are shown in Table S1. The chars were physically activated with CO_2 in a vertical furnace. Each sample was placed into a quartz crucible suspended from a thermobalance and heated to 900 °C under nitrogen flow at a rate of 10 °C min^{-1}. Once this temperature was reached, the nitrogen flow was switched to a pure CO_2 flow of 20 dm^3 h^{-1}. The burn-off of 50, 70, and 70 wt% was applied for the Ch1, Ch2, and Ch3 chars, respectively, in order to obtain carbons with comparable microporous structures. The resulting ACs were labeled as NCh1, NCh2, and NCh3.

2.2 Characterization

The porous structure of the ACs was examined by N_2 adsorption at 77 K using an Autosorb IQ gas sorption analyzer (Quantachrome). The specific surface area was calculated using the BET equation. The amount of nitrogen adsorbed at a relative pressure of $p/p_0 = 0.96$ was used to determine the total pore volume (V_T). The micropore volume (V_{DR}) was estimated from the Dubinin–Radushkevich equation. The mesopore volume (V_{mes}) was calculated as the difference between V_T and V_{DR}. The pore size distribution was also calculated from the isotherm data by applying the Quenched-solid density functional theory method (QSDFT) [30]. The crystalline properties of the materials were studied by X-ray diffraction (XRD) using an Ultima IV Rigaku analyzer equipped with a 2 kW X-ray tube (40 kV per 30 mA) using Cu Kα2 radiation ($\lambda = 1.54056$ Å). The elemental determination of the C, H, N, and S contents was achieved using a Vario MICRO cube analyzer, and the oxygen content was directly measured using a Carlo Erba EA 1108 Elemental Analyzer. The XPS measurements were performed on a PHI 5000 VersaProbe apparatus to determine the concentrations of nitrogen and oxygen and their distribution on the surface. The N1s core-level spectra were resolved into four individual peaks that represent pyridine N-oxide (NX, B.E. = 402–405 eV), quaternary nitrogen (NQ, BE = 401.4 eV), pyrrolic and pyridonic groups (N-5, BE = 400.3 eV), and pyridinic groups (N-6, BE = 398.7 eV) [31]. The O1s spectra included quinone (O-I, BE = 530.6 eV), hydroxyl, ester, ether, and anhydride (O-II, BE = 532.0 eV) groups, and adsorbed water and oxygen molecules (O-III, BE = 535.8 eV) [32]. Curve fitting was performed by an iterative least squares algorithm (CasaXPS software) using a Gaussian–Lorentzian (70/30) peak shape and applying the Shirley background correction.

2.3 Electrochemical measurements

Disk-type electrodes were prepared by mixing 85 wt% of each AC (active material) with 5 wt% of acetylene carbon black and 10 wt% of the binder polyvinylidene fluoride (PVDF, Kynar Flex 2801). The pellets had a geometric surface area of 0.9 cm^2 and a thickness of ~0.2 mm. Two- and three-electrode capacitors were assembled in Swagelok® systems with pellets of comparable mass (8–10 mg). The electrodes were separated by a glassy fibrous paper. The measurements were performed in an aqueous solution consisting of 1 M H_2SO_4 using gold current collectors to avoid corrosion and preserve comparable experimental conditions. The potentiostat–galvanostat VSP Biologic (France) was employed to determine the electrochemical properties of the ACs. In the three-electrode cell, cyclic voltammetry measurements were performed at a voltage range of −0.57 to 0.23 V and a scan rate in the range of 0.2–100 mV s^{-1} using Hg/Hg_2SO_4 as a reference electrode. The measurements in the two-electrode symmetric system were performed by cyclic voltammetry at a

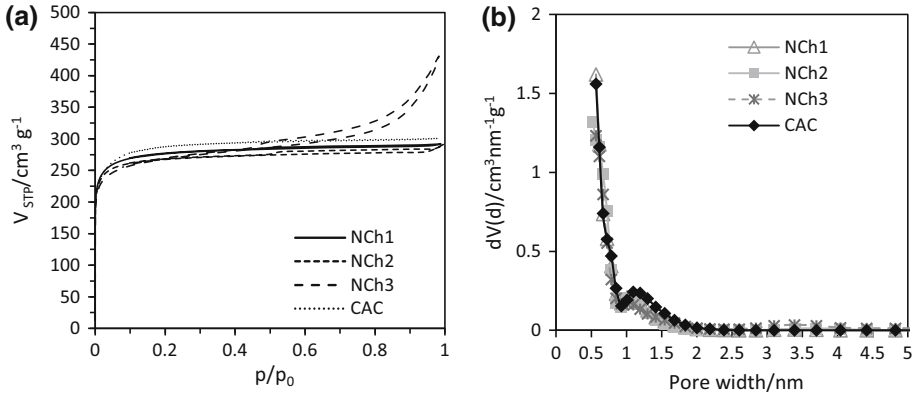

Fig. 1 Adsorption isotherms of nitrogen at 77 K (**a**) and QSDFT pore size distributions for the ACs (**b**)

voltage scan rate of 1–100 mV s^{-1}, galvanostatic cycling at current densities from 0.2 to 20 A g^{-1} in a potential range of 0–0.8 V, and electrochemical impedance spectroscopy in the frequency range from 10 mHz to 100 kHz. The capacitance was expressed in farads per mass of active material or farads per specific surface area in one electrode. The specific capacitance values (C, F g^{-1}) were calculated from the CV curves and the galvanostatic discharge curves according to Eqs. (1) and (2), respectively.

$$C = \frac{\int I\mathrm{d}t}{vm_{\mathrm{el}}}, \tag{1}$$

$$C = \frac{\int I\mathrm{d}t}{Um_{\mathrm{el}}}, \tag{2}$$

where I (A) is the current, t (s) is the time, v (V s^{-1}) is the scan rate, U (V) is the operating cell voltage, and m_{el} (g) is the mass of the active material in one electrode. The energy density (E, Wh kg^{-1}) and power (P, W kg^{-1}) were calculated using the following equations:

$$E = \frac{1}{2}CU^2, \tag{3}$$

$$P = \frac{E}{\Delta t_{\mathrm{dis}}}, \tag{4}$$

where Δt_{dis} is the discharge time.

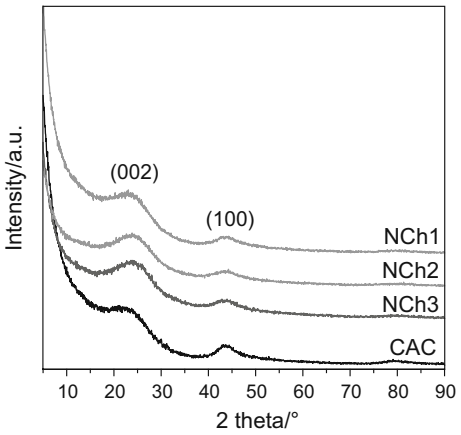

Fig. 2 XRD patterns of the studied ACs

3 Results and discussion

3.1 Structural and chemical characterization

The chitosan chars, containing 8.8–9.8 wt% of nitrogen, were physically activated to produce the ACs with a well-developed microporous structure. The experimental conditions for the activation of the various chitosan chars were adjusted to obtain chitosan-based ACs with similar microporous textures. For comparative purposes, the

Table 1 Textural parameters and elemental composition of the ACs

Sample	Textural parameters					Elemental composition (wt%)				
	S_{BET} (m^2 g^{-1})	V_{T} (cm^3 g^{-1})	V_{DR} (cm^3 g^{-1})	V_{mes} (cm^3 g^{-1})	L_0 (nm)	C	H	N	S	O
NCh1	1080	0.45	0.41	0.04	0.79	90.8	0.8	5.4	0.0	3.0
NCh2	1054	0.45	0.40	0.05	0.76	88.3	1.0	5.0	0.0	5.7
NCh3	1022	0.65	0.40	0.25	0.83	86.6	1.4	3.6	0.0	8.4
CAC	1101	0.46	0.42	0.04	0.95	95.3	1.4	0.1	0.0	3.3

S_{BET} specific surface area; V_{T} total pore volume; V_{DR} micropore volume; V_{mes} mesopore volume; L_0 average micropore diameter

commercial activated carbon Berkosorb® (named CAC), with a negligible nitrogen content (0.1 wt%) and comparable textural properties, was also included in this study.

The adsorption/desorption isotherms of nitrogen at 77 K for the chitosan-based ACs and CAC are shown in Fig. 1a. The curve obtained for NCh3 was of type IV, which is typical of microporous carbons that also contain mesopores. For the other samples, the isotherms were of type I, which is characteristic of primarily microporous carbons. The amount of nitrogen adsorbed at low relative pressures is similar in all of the tested samples, which is indicative of their comparable microporosities. At high relative pressures, further adsorption of nitrogen was observed for NCh3, as well as a small hysteresis loop, which is associated with capillary condensation in the mesopores. The textural properties of the chitosan-based ACs and CAC, which were calculated from the nitrogen-adsorption isotherms, are listed in Table 1. The chitosan-based ACs exhibit comparable specific surface areas (S_{BET}) of 1022–1080 $m^2\ g^{-1}$ and micropore volumes (V_{DR}) of 0.40–0.41 $cm^3\ g^{-1}$. A higher total pore volume was observed in NCh3 (0.65 $cm^3\ g^{-1}$ for NCh3 and 0.45–0.46 $cm^3\ g^{-1}$ for the rest) due to the relatively higher presence of mesopores. All the samples showed a similar bimodal distribution of micropore sizes (Fig. 1b), which agrees with their similar nitrogen uptake at low relative pressures. A local maximum was detected at a pore size of 1.1 nm, with almost the same intensity in all samples. The XRD patterns of CAC and the N-doped carbons are shown in Fig. 2. Two broad diffraction peaks, ascribed to 002 and 100 planes, can be observed for all ACs. The low intensity of the 002 diffraction peak indicates a poorly ordered graphitic structure in all the samples.

The elemental composition of the ACs, which was determined by elemental analysis, is included in Table 1. The chitosan-based ACs exhibit different nitrogen and oxygen contents. In general, a decrease in the nitrogen content was observed with an increase in the oxygen content. Therefore, NCh1 was characterized by the highest nitrogen content (5.4 wt%) and the lowest oxygen content (3.0 wt%). In contrast, sample NCh3 has the lowest nitrogen content (3.6 wt%) and the highest oxygen content (8.4 wt%). Importantly, the nitrogen content in CAC was negligible.

The surface chemistry of the ACs was studied using X-ray photoelectron spectroscopy (XPS). The XPS results

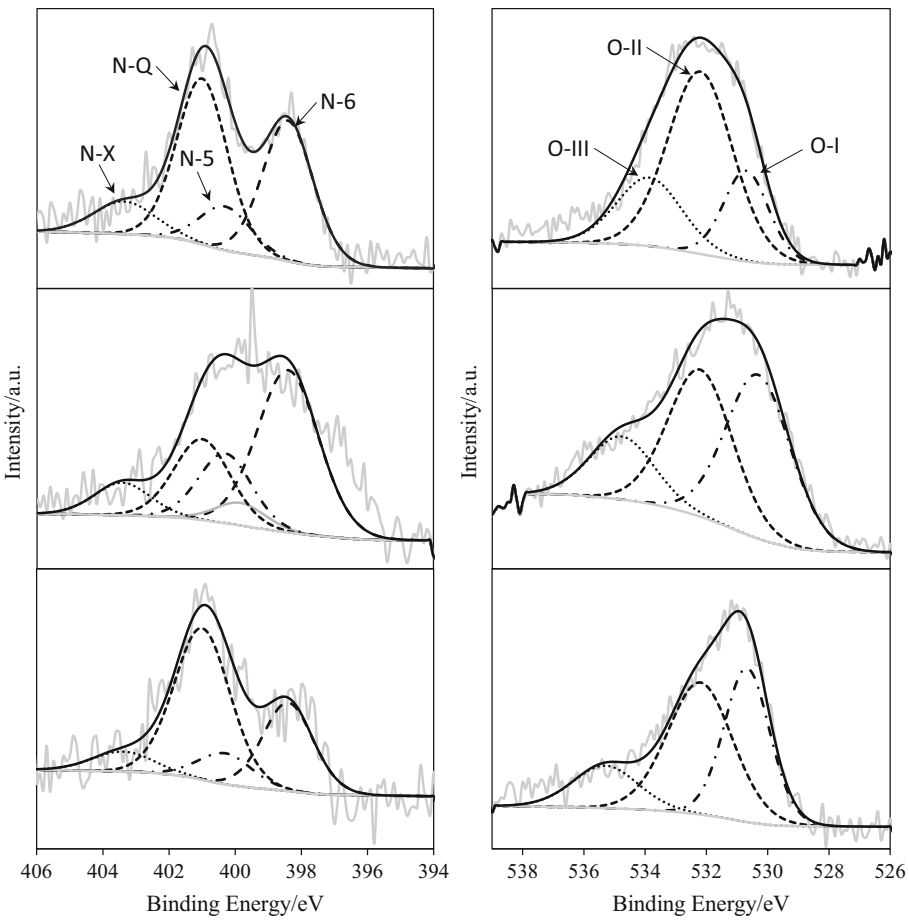

Fig. 3 N1s (*left*) and O1s (*right*) XPS spectra of the chitosan-based ACs

Table 2 Elemental composition (XPS) and relative abundance of nitrogen and oxygen functional groups, determined by deconvolution of the N1s and O1s core-level spectra

Sample	C (at.%)	N (at.%)	O (at.%)	N1s deconvolution (%)				O1s deconvolution (%)		
				N-6	N-5	N-Q	N-X	O-I	O-II	O-III
NCh1	90.4	3.9	5.7	38	12	44	6	20	58	22
NCh2	87.6	3.8	8.6	43	35	17	5	44	39	17
NCh3	91.0	1.9	7.1	29	11	55	5	38	47	15

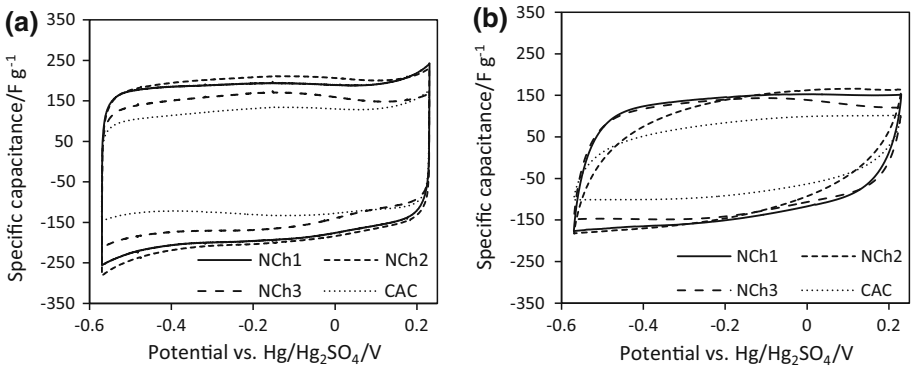

Fig. 4 Cyclic voltammetry curves for the ACs in the three-electrode system at scan rates of 0.5 mV s^{-1} (**a**) and 100 mV s^{-1} (**b**)

indicated a lower nitrogen content and higher oxygen content on the surface of the activated samples compared to the results obtained from elemental analysis (in reference to the bulk material), due to the evolution of nitrogen and oxygen fixation occurring during the activation step. The nature of the nitrogen on the surface of the chitosan-based ACs was determined based on the deconvolution of the N1 s core-level spectra, which are shown in Fig. 3 (left). In NCh1 and NCh3, quaternary nitrogen (N-Q) is the most abundant type of nitrogen with contributions of 44 and 55 %, respectively, to the total nitrogen-containing groups (Table 2). However, sample NCh2 has the highest contribution of pyridinic-N (N-6) and pyrrolic-N (N-5) groups (43 and 35 %, respectively). The distribution of oxygen functionalities was also studied by deconvolution of the O1s core-level XPS spectra (Fig. 3, right). The main difference observed was the low content of quinone-O (O-I) in NCh1, with a contribution of 20 % to the O1s peak, in comparison with NCh2 and NCh3, whose abundances of this oxygen group were 44 and 38 %, respectively.

3.2 Electrochemical performance

Cyclic voltammetry enables the determination of the faradaic and non-faradaic behaviors of the electrode materials, as well as estimation of the specific capacitance values. Figures 4a and b show the CV curves of the ACs at low (0.5 mV s^{-1}) and high (100 mV s^{-1}) scan rates. respectively. At 0.5 mV s^{-1}, the curves have an almost rectangular shape, which confirms the good conductivity and fast charge propagation in the tested materials. The chitosan-based ACs exhibited very high capacitances of 194, 205, and 168 F g^{-1} for NCh1, NCh2, and NCh3, respectively. Despite having a comparable BET surface area, the capacitance value for CAC at 0.5 mV s^{-1} was only 132 F g^{-1}.

The N-enriched samples exhibit superior capacitive behavior compared to that of CAC. As previously mentioned, all of the samples have comparable BET surface areas and micropore volumes (Table 1). Therefore, the differences in their capacitance values must be related to their chemical composition. At low scan rates, the presence of broad, reversible humps in a potential range between −0.3 and 0 V was identified in all of the samples, confirming the co-contribution of a high electrical double-layer capacitance and pseudocapacitance due to the presence of nitrogen and oxygen moieties in the ACs. At low scan rates, NCh2 exhibits the highest capacity value, which agrees with the highest total content of nitrogen- and oxygen-containing functional groups on its surface, based on the XPS results (Table 2). In addition, this sample possesses the highest content of pyridinic-N (N-6), pyrrolic/pyridonic-N (N-5), and quinone-O (O-I) groups, to whom the pseudocapacitive effect is attributed [33, 34]. Hydroxyl groups were also found to contribute to pseudocapacitance [35]. However, the contribution of other oxygen groups as ethers, esters, or anhydrides is also ascribed to the peak at 532 eV (O-II) and, therefore, the individual effect of hydroxyl groups could not be assessed. The heteroatom content is lower in NCh1 and NCh3, and therefore, their capacitance values are also lower. The low capacitance value observed for CAC was due to the

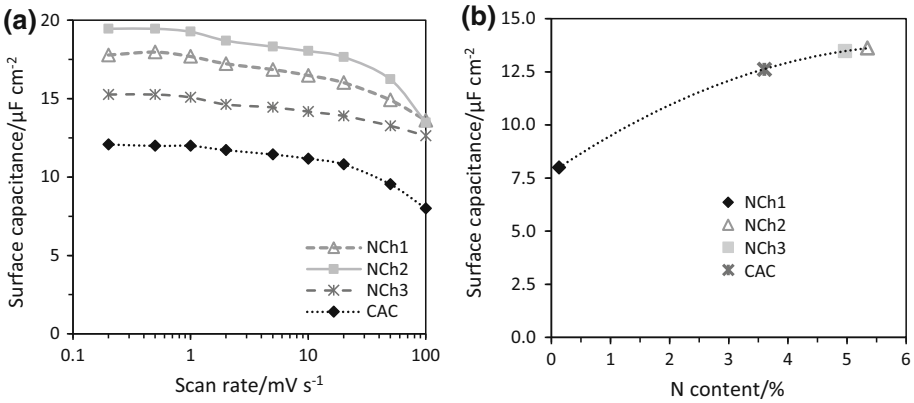

Fig. 5 Surface capacitance in the three-electrode system as a function of the scan rate (**a**) and normalized capacitance values at 100 mV s^{-1} as a function of the N content (**b**)

absence of nitrogen and its low oxygen content (3.3 wt%). According to previous studies, the presence of nitrogen moieties increases the electronic charge density on the surface of the ACs, which favors the adsorption of protons from the acidic electrolyte [16, 36]. Therefore, the presence of nitrogen functionalities in the chitosan-based ACs may have enhanced their pseudocapacitive behavior, as well as their double-layer capacitance.

All of the N-enriched samples maintain very high capacitance values in the range of 139–147 F g^{-1} at a high scan rate of 100 mV s^{-1}. At the same scan rate, CAC exhibits a lower capacitance value of 86 F g^{-1}. The high capacitance values that are maintained by the chitosan-based ACs at a high scan rate confirm the favorable charge transport in these samples. Although the presence of mesopores may be related to the improved electrochemical behavior [2, 37], no relevant enhancement in the charge transport was observed for the mesopore-enriched NCh3 compared to the other chitosan-based samples. Therefore, the improved electrochemical performance of NCh3 compared to CAC appears to be related to the presence of nitrogen rather than to a higher contribution of mesopores. The relationship between the capacitance per specific surface area and the scan rate is plotted in Fig. 5a. The chitosan-based ACs exhibited very high surface capacitance values (up to 19.5 μF cm^{-2}) and high capacity retentions at 100 mV s^{-1} for NCh1 and NCh3 (77 and 83 %, respectively). These samples are characterized by a higher content of quaternary-N (Fig. 3, Table 2), which exists as positively charged groups that enhance electron transfer at high scan rates. It is remarkable that the surface capacitance values of the ACs obtained from chitosan by activation with CO_2 are almost twice as high as those of highly porous chitosan-based KOH from the same precursor [27]. This feature is very desirable from the point of view of implementing porous carbon materials as supercapacitor electrode.

The superior charge propagation of NCh1 and NCh3 was confirmed by the rectangular shape observed in their CV curve at a scan rate of 100 mV s^{-1} (Fig. 4b). In contrast, NCh2 exhibits the lowest capacity retention (69 %), which is comparable to that observed for CAC (66 %). This feature may be due to its lower contribution of quaternary-N (17 %). However, NCh2 has much better capacitive behavior than CAC, despite having a similar porous texture and oxygen content (Table 1), which confirms the favorable effect of nitrogen on the electrochemical performance. The overall effect of the nitrogen content

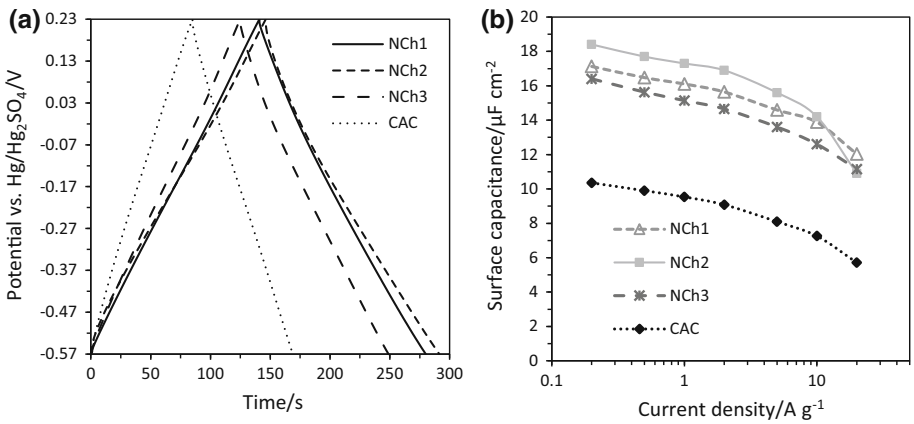

Fig. 6 Galvanostatic charge/discharge curves for the ACs in the three-electrode system at a current density of 1 A g^{-1} (**a**) and surface capacitance as a function of the current density (**b**)

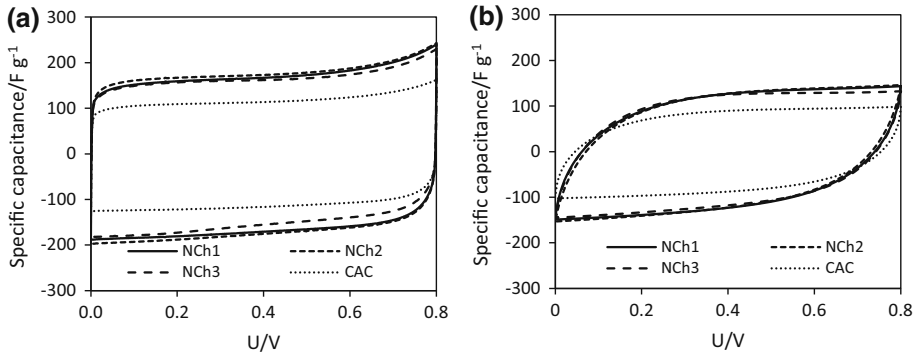

Fig. 7 Cyclic voltammetry curves in a symmetric system for the ACs at scan rates of 1 mV s^{-1} (**a**) and 100 mV s^{-1} (**b**)

(i.e., comprising both enhanced capacitance and charge propagation) is shown in Fig. 5b, where the surface capacitance at 100 mV s^{-1} is plotted as a function of the bulk nitrogen content. The positive correlation observed confirms the enhanced capacitive behavior of the N-enriched chitosan-based ACs at high scan rates.

The galvanostatic charge and discharge curves obtained for the studied ACs at 1 A g^{-1} are presented in Fig. 6a. The shape of the charge/discharge curves is triangular and symmetric, indicating that the predominant storage mechanism is the double-layer formation. A small distortion of charge and discharge curves related to the contribution of pseudocapacitance was observed in the case of NCh2, which is in accordance with its high contents of pyridinic and pyrrolic/pyridonic groups. The capacitance values of N-enriched samples are significantly higher than those obtained for the non-doped carbon. For CAC, the capacitance value was 114 at 0.2 A g^{-1} and it dropped to 63 F g^{-1} at 20 A g^{-1}. The chitosan-based ACs exhibited an almost twice higher capacitance in the entire current density range, reaching 194 F g^{-1} at 0.2 A g^{-1}. The high specific capacitance of N-enriched carbons and their relatively low specific surface area ($\sim$1000 m^2 g^{-1}) imply a very high surface capacitance of 15–18 μF g^{-1} at 1 A g^{-1}, while it was only 9.5 μF g^{-1} for CAC (Fig. 6b).

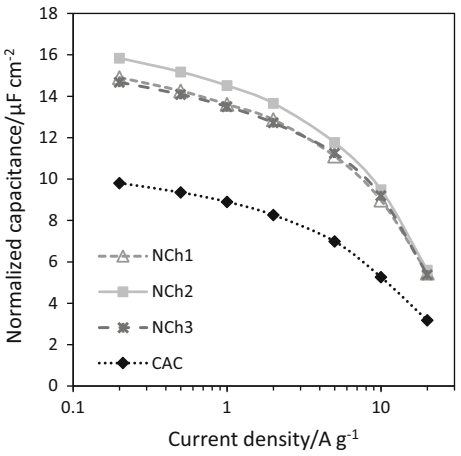

Fig. 8 Normalized capacitance in a symmetric system as a function of the current density

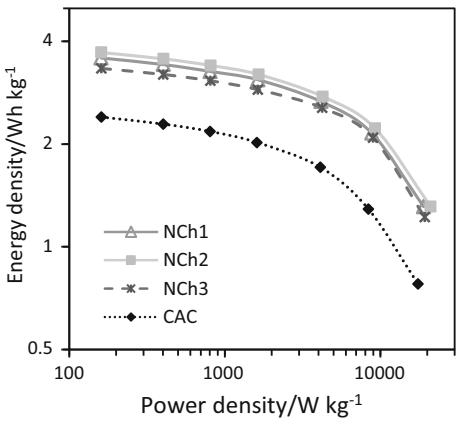

Fig. 9 Ragone plot of the chitosan-based and commercial ACs

The electrochemical behavior of the chitosan-based ACs was also studied in a two-electrode symmetric system using cyclic voltammetry and galvanostatic charge/discharge measurements. The cyclic voltammograms at low (1 mV s^{-1}) and high (100 mV s^{-1}) scan rates are shown in Fig. 7. In agreement with the measurements in the three-electrode cells, the chitosan-based ACs exhibit enhanced capacitance at both low and high scan rates, compared to the commercial CAC with a similar surface area. The differences in the behavior of the chitosan-based ACs are much smaller than those observed in the three-electrode systems. Only a slightly lower capacitance was observed for the capacitor constructed with NCh3, which was characterized by the lowest heteroatom content. Other authors described the preparation, through multistep and time-consuming procedures, of nitrogen-enriched materials with lower capacitance values and poorer capacity retentions at high scan rates [10, 18, 20, 33]. To the best of our knowledge, the superior electrochemical behavior exhibited by the chitosan-based materials has not been achieved without the use of nitrogenized additives or additional treatments.

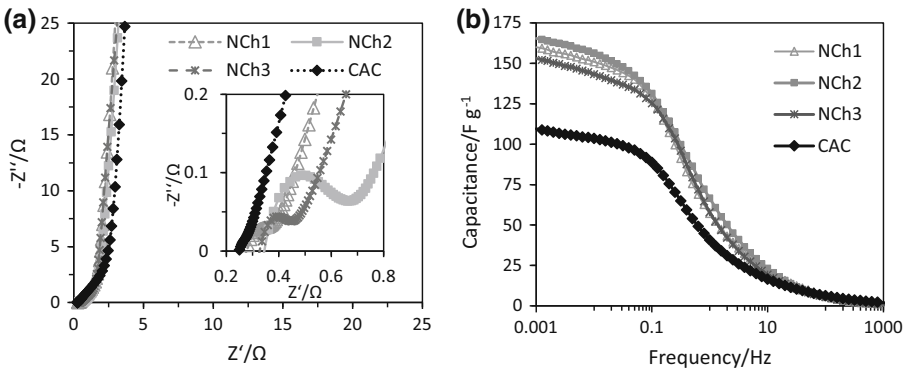

Fig. 10 Nyquist plots (**a**) and specific capacitance as a function of the frequency (**b**) for the chitosan-based and commercial ACs

The relationship between the normalized capacitance and the applied current density for a two-electrode system is plotted in Fig. 8. In the entire current density range, the normalized capacitance of the chitosan-based ACs is higher than that observed for CAC. At low current densities, the capacitance of NCh2 is slightly higher than that of NCh1 and NCh3. However, NCh1 and NCh3 exhibit a higher capacity retention, and the capacitance values of the three chitosan-based ACs are similar at the highest current density. This observation is consistent with the measurements using the three-electrode cells. Moreover, the comparison of the energy power characteristics (Ragone plot) of the nitrogen-doped ACs and the non-doped AC (Fig. 9) demonstrates clearly the positive impact of nitrogen functionalities on the capacitor performance.

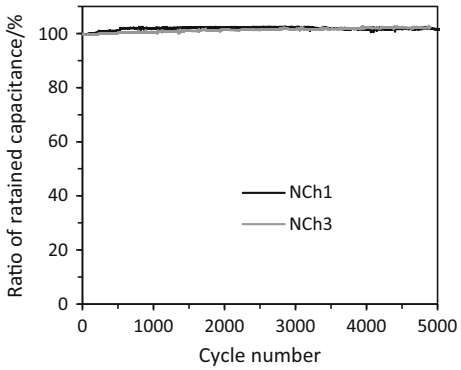

Fig. 11 Cycling stability of NCh1 and NCh3 at a current density of 1 A g^{-1}

Electrochemical impedance spectroscopy of the ACs, measured in a symmetric cell, is shown in Fig. 10a in the form of a Nyquist plot. The ESR values at 100 kHz were very low for all of the tested materials (0.25–0.35 Ω), and the differences between these values were negligible. The presence of semicircles at high frequencies in the Nyquist plots of the N-ACs confirms the pseudocapacitance effect observed for these samples. NCh2 showed the largest semicircle, which is in agreement with its highest content of pyrrolic and pyridinic groups. Smaller semicircles were detected in the high frequency region of NCh1 and NCh3, according to their lower pseudocapacitive behavior compared to NCh2. In the case of CAC, the semicircle was not observed despite the presence of oxygen groups (3 wt%) in its structure. The impedance in the middle frequency range provides information about ion-diffusion resistance in the porous structure of the ACs [38]. Despite having a slightly larger average micropore size (Table 1), CAC exhibits a higher diffusion resistance compared with N-ACs. This effect is due to better ion transport in the pores of the

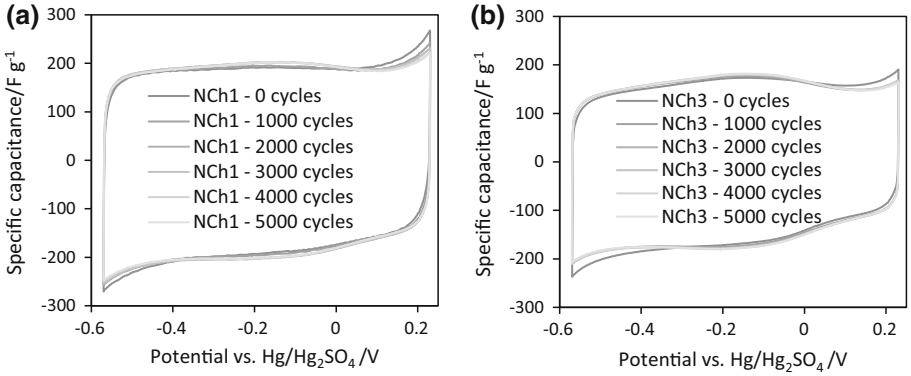

Fig. 12 Cyclic voltammetry curves of NCh1 (**a**) and NCh3 (**b**) at 0.5 mV s^{-1} after various cycles

chitosan-based ACs, resulting from the presence of nitrogen, which confers a better wettability and enhanced basicity to the surface [18, 35]. The specific capacitance as a function of the frequency is plotted in Fig. 10b. For all of the samples, a nearly vertical line was observed at low frequencies, which is indicative of their purely capacitive behavior. As the frequency increases, the capacitance values decrease due to the ion-diffusion restriction in the pores. The N-enriched chitosan-based ACs exhibit superior performance compared to that of the nearly N-free CAC, which is consistent with the results obtained from cyclic voltammetry measurements.

For practical application, the cycling stability must be confirmed for each electrode material, especially for those with pseudocapacitance [2]. To investigate the cycling stability of the materials, galvanostatic charge/discharge cycling was applied to the three-electrode cells at a current density of 1 A g^{-1} in a voltage range of −0.57 to 0.23 V vs. Hg/Hg_2SO_4. Figure 11 shows the retained capacitance during 5000 cycles for the chitosan-based ACs with the highest and lowest nitrogen contents (NCh1 and NCh3, respectively): 100 % of the original value was maintained over the entire experiment for both samples. This excellent cycling stability indicates that the nitrogen and oxygen functional groups responsible for the reversible faradaic reactions are strongly bonded to carbon, which result in stability during long cycling. Figure 12 shows the CV curves obtained for NCh1 and NCh3 before cycling and after 1000, 2000, 3000, 4000, and 5000 cycles. The preservation of the rectangular shape observed during the entire cycling test confirms that the superior charge propagation was maintained after long cycling.

4 Conclusions

Chitosan-based ACs with various nitrogen contents and distributions were obtained by the physical activation of chitosan chars. A comparative study of chitosan-based carbons and a commercial AC with a similar microporous structure confirmed the important role of nitrogen in the capacitive behavior. In general, the performance of the N-containing chitosan-based carbons was superior to that of the commercial AC. The contribution of pseudocapacitance due to the presence of pyridinic and pyrrolic, as well as quinone, groups was detected at low scan rates. All of the N-containing carbons exhibited very high capacitance values (139–147 F g^{-1}) at a high scan rate of 100 mV s^{-1}, and the carbons with the highest content of quaternary nitrogen (NCh1 and NCh3) exhibited the highest rate capability. The high stability of the nitrogen groups led to the excellent cyclability of the chitosan-based ACs, which maintained 100 % of their initial capacitance over 5000 charge/discharge cycles. Therefore, the physical activation of chitosan-based chars is suitable for the preparation of porous carbons with a high nitrogen content. The limited surface area provided by the physical activation is substantially compensated by the pseudocapacitive effect and enhanced conductivity supplied by the presence of nitrogen, especially in the high-rate regime. Due to their good capacitive behavior and excellent stability, chitosan-based ACs exhibit promising applicability as electrode materials for energy storage in supercapacitors.

Acknowledgments This work was financed by a statutory activity subsidy from the Polish Ministry of Science and Higher Education for the Faculty of Chemistry of Wrocław University of Technology. The authors wish to thank Mazovia Center for Surface Analysis at the Institute of Physical Chemistry of the Polish Academy of Science in Warsaw.

References

1. Kötz R, Carlen M (2000) Principles and applications of electrochemical capacitors. Electrochim Acta 45:2483–2498
2. Pandolfo AG, Hollenkamp AF (2006) Carbon properties and their role in supercapacitors. J Power Sources 157:11–27
3. Gryglewicz G, Śliwak A, Béguin F (2013) Carbon nanofibers grafted activated carbon as electrode of high power supercapacitors. ChemSusChem 6:1516–1522
4. Raymundo-Piñero E, Kierzek K, Machnikowski J, Béguin F (2006) Relationship between the nanoporous texture of activated carbons and their capacitance properties in different electrolytes. Carbon 44:2498–2507
5. Xue R, Yan J, Liu X, Tian Y, Baolian Y (2011) Effect of activation on the carbon fibers phenol-formaldehyde resins for electrochemical supercapacitors. J Appl Electrochem 41:1357–1366
6. Kierzek K, Frąckowiak E, Lota G, Gryglewicz G, Machnikowski J (2004) Electrochemical capacitors based on highly porous carbons prepared by KOH activation. Electrochim Acta 49:515–523
7. Béguin F, Presser V, Balducci A, Frąckowiak E (2014) Carbons and electrolytes for advanced supercapacitors. Adv Mater 26:2219–2251
8. Gryglewicz G, Machnikowski J, Lorenc-Grabowska E, Lota G, Frąckowiak E (2005) Effect of pore size distribution of coal-based activated carbons on double layer capacitance. Electrochim Acta 50:1197–1206
9. Wang J, Kaskel S (2012) KOH activation of carbon-based materials for energy storage. J Mater Chem 22:23710–23725
10. Hulicova D, Kodama M, Hatori H (2006) Electrochemical performance of nitrogen-enriched carbons in aqueous and non-aqueous supercapacitors. Chem Mater 18:2318–2326
11. Kim ND, Kim W, Joo JB, Oh S, Kim P, Kim Y, Yi J (2008) Electrochemical capacitor performance on N-doped mesoporous

carbons prepared by ammoxidation. J Power Sources 180:671–675
12. Lota G, Fic K, Frackowiak E (2011) Carbon nanotubes and their composites in electrochemical applications. Energy Environ Sci 4:1592–1605
13. Starck J, Burg P, Muller S, Bimer J, Furdin G, Fioux P, Guterl CV, Begin D, Faure P, Azambre B (2006) The influence of mineralization and ammoxidation on the adsorption properties of an activated carbon prepared from polish lignite. Carbon 44:2549–2557
14. Jurewicz K, Babeł K, Ziółkowski A, Wachowska H (2003) Ammoxidation of active carbons for improvement of supercapacitor characteristics. Electrochim Acta 48:1491–1498
15. Świetlik U, Grzyb B, Torchała K, Gryglewicz G, Machnikowski J (2014) High temperature ammonia treatment of pitch particulates and fibers for nitrogen enriched microporous carbons. Fuel Process Technol 119:211–217
16. Seredych M, Hulicova-Jurcakova D, Lu GQ, Bandosz TJ (2008) Surface functional groups of carbons and the effects of their chemical character, density and accessibility to ions on electrochemical performance. Carbon 46:1475–1488
17. Shen W, Fan W (2013) Nitrogen-containing porous carbons: synthesis and application. J Mater Chem A 1:999–1013
18. Frąckowiak E, Lota G, Machnikowski J, Vix-Guterl C, Béguin F (2006) Optimisation of supercapacitors using carbons with controlled nanotexture and nitrogen content. Electrochim Acta 51:2209–2214
19. Gliścińska E, Babeł K (2013) Preparation of activated carbon fibres from electrospun polyacrylonitrile fibre mat and characterization of their chemical and structural properties. Fibres Text East Eur 99:42–47
20. Lota G, Grzyb B, Machnikowska H, Machnikowski J, Frąckowiak E (2005) Effect of nitrogen in carbon electrode on the supercapacitor performance. Chem Phys Lett 404:53–58
21. Ra EJ, Raymundo-Piñero E, Lee YH, Béguin F (2009) High power supercapacitors using polyacrylonitrile-based carbon nanofiber paper. Carbon 47:2984–2992
22. Torchała K, Kierzek K, Gryglewicz G, Machnikowski J (2015) Narrow-porous pitch-based carbon fibers of superior capacitance properties in aqueous electrolytes. Electrochim Acta 167:348–356
23. Kishore B, Shanmughasundaram D, Penki TR, Munichandraiah N (2014) Coconut kernel-derived activated carbon as electrode material for electrical double-layer capacitors. J Appl Electrochem 44:903–916
24. Kucińska A, Cyganiuk A, Łukaszewicz JP (2012) A microporous and high surface area activated carbon obtained by the heat-treatment of chitosan. Carbon 50:3092–3116
25. Fan X, Zhang L, Zhang G, Shu Z, Shi J (2013) Chitosan derived nitrogen-doped microporous carbons for high performance CO_2 capture. Carbon 61:423–430
26. Łukaszewicz JP, Kucińska A, Gołembiewski R (2014) Synthesis of N-rich activated carbons from chitosan by chemical activation. Sci Adv Mater 6:290–297
27. Wróbel-Iwaniec I, Díez N, Gryglewicz G (2015) Chitosan-based highly activated carbons for hydrogen storage. Int J Hydrog Energy 40:5788–5796
28. Hu Y, Wang H, Yang L, Liu X, Zhang B, Liu Y, Xiao Y, Zheng M, Lei B, Zhang H, Fu H (2013) Preparation of chitosan-based activated carbon and its electrochemical performance for EDLC. J Electrochem Soc 6:H321–H326
29. Gao F, Qu J, Zhao Z, Wang Z, Qiu J (2016) Nitrogen-doped activated carbon derived from prawn shells for high-performance supercapacitors. Electrochim Acta 190:1134–1141
30. Neimark AV, Lin Y, Ravikovitch PI, Thommes M (2009) Quenched solid density functional theory and pore size analysis of micro-mesoporous carbons. Carbon 47:1617–1628
31. Pietrzak R (2009) XPS study and physico-chemical properties of nitrogen-enriched microporous activated carbon from high volatile bituminous coal. Fuel 88:1871–1877
32. Fan X, Yu Ch, Yang J, Ling Z, Qiu J (2014) Hydrothermal synthesis and activation of graphene-incorporated nitrogen-rich carbon composite for high-performance supercapacitors. Carbon 70:130–141
33. Hulicova-Jurcakova D, Seredych M, Lu GQ, Bandosz TJ (2009) Combined effect of nitrogen- and oxygen-containing functional groups of microporous activated carbon on its electrochemical performance in supercapacitors. Adv Func Mater 19:438–447
34. Jeong HM, Lee JW, Shin WH, Choi YJ, Shin HJ, Kang JK, Choi JW (2011) Nitrogen-doped graphene for high-performance ultracapacitors and the importance of nitrogen-doped sites at basal planes. Nano Lett 11:2472–2477
35. Śliwak A, Grzyb B, Ćwikła J, Gryglewicz G (2013) Influence of wet oxidation of herringbone carbon nanofibers on the pseudocapacitance effect. Carbon 64:324–333
36. Lee YH, Chang KH, Hu ChCh (2013) Differentiate the pseudocapacitance and double-layer capacitance contributions for nitrogen-doped reduced graphene oxide in acidic and alkaline electrolytes. J Power Sources 227:300–308
37. Lv Y, Zhang F, Dou Y, Zhai Y, Wang J, Liu H, Xia Y, Tu B, Zhao D (2012) A comprehensive study on KOH activation of ordered mesoporous carbons and their supercapacitor application. J Mater Chem 22:93–99
38. Zhou M, Pu F, Wang Z, Guan S (2014) Nitrogen-doped porous carbons through KOH activation with superior performance in supercapacitors. Carbon 68:185–194